Theor Chim Acta (1987) 72: 433–458

Theoretica Chimica Acta

Charge density topological study of bonding in lithium clusters*

Part I: Planar Li_n clusters ($n = 4, 5, 6$)

Carlo Gatti[1], Piercarlo Fantucci[2] and Gianfranco Pacchioni[2]

[1] Centro CNR "Relazioni fra Struttura e Reattivita' Chimica", via Golgi 19, I-20133 Milano, Italy

[2] Dipartimento di Chimica Inorganica e Metallorganica, Centro CNR, Universita' di Milano, via Venezian 21, I-20133 Milano, Italy

(Received June 5; revised and accepted September 2, 1987)

The topological behaviour of the electron density (ρ) derived from correlated wavefunctions is analyzed for Li_2, $Li_4(D_{2h})$, $Li_5(C_{2v})$, and $Li_6(D_{3h})$ planar clusters considered in their optimal geometry. The topology of ρ of Li_2 shows an unusual maximum located at the midpoint of the Li–Li equilibrium distance. The occurrence of maxima of ρ at positions other than nuclei (characteristic also for planar Li_4, Li_5, and Li_6 clusters) implies the existence of molecular subspaces (bounded by zero-flux surfaces in the gradient of ρ at each point of the surface) which do not enclose a nucleus but still satisfy the virial theorem. This result provides a generalization of Bader's quantum theory of atoms in molecules to systems in which electrons behave partially as mobile metallic electrons. Maxima of ρ preferentially occur within the triangles (two in Li_4, two in Li_5 and three in Li_6), while the number of maxima at the Li–Li midpoint is minimized: they are present only when the existence of a maximum within a triangle is not allowed because of the non suitable formal valence of the Li atoms involved. All the cluster atoms are bonded to "attractors" associated with the unusual ρ maxima, but they are not directly bonded to each other. The cluster stability is found to be dependent on the number and kind of ρ maxima. The topological analysis clearly differentiates between Li atoms which occupy different coordination positions within the cluster in terms of their local and average properties. In particular, the degree of *sp* hybridization is markedly different for Li atoms with two, three or four nearest neighbors. This implies that a unique definition of a reference valence state for atoms in clusters is impossible. As a consequence, the use of standard electron density difference maps for the description of the charge accumulation and depletion process which ensues the chemical bonding, appears rather questionable.

Key words: Lithium clusters — Metallic bond — Charge density topology

* Dedicated to Professor J. Koutecký on the occasion of his 65th birthday

1. Introduction

In the recent years the problem of the electronic structure of metal clusters has challenged the interest of several research groups [1, 2]. While accurate studies on transition metal clusters are scarce, due to obvious theoretical and computational difficulties, the field of light atom clusters has been successfully investigated also with advanced quantum mechanical methods. In this context, the alkali metal clusters represent a very special case: systematic investigations have been carried out with different methodologies and, quite interestingly, a general agreement has been reached as for the optimal geometry of Li_n and Na_n clusters, at least of those of low nuclearity ($n < 8$) [3–10].

The available results allow one to formulate few general rules governing the cluster stability and the topology involved in the cluster growth [11]. These rules, applied to the case of the Li_n clusters, can be summarized as follows: (i) the *p* polarization functions on each Li center play a crucial role in determining both the basic geometry and the stability of the clusters. The involvement of 2*p* atomic orbitals is an indication of a partial *sp* hybridization, to an extent which markedly depends upon the particular situation (coordination number, surface or bulk character) of each lithium atom; (ii) for a given cluster nuclearity the most stable forms often are not the most symmetric ones, due to the occurence of Jahn–Teller distortions; (iii) up to Li_6, the most stable cluster geometries are planar, being composed of equilateral (or slightly deformed) triangles [10, 12]. Li_6 in its planar D_{3h} form is nearly degenerate with the pentagonal pyramid (C_{5v}) [10, 13, 14]. The Li_6 cluster represents the transition point from planar to three-dimensional structures (the most favorable for clusters of higher nuclearity) which are built from basic tetrahedral units [10, 15].

Some of the aspects connected with the above mentioned rules have evident effects on the global electron density of the cluster which has been analyzed on the basis of orbital densities [15], total densities [8, 10] or electron difference maps (EDM) [10, 16]. However, no quantitative analysis of the spatial behaviour of the charge density has so far been attempted. Moreover, the EDMs obtained by subtracting the spherical densities of the constituent (non interacting) atoms may be in error when the bond formation is accompanied by an important *sp* hybridization [17], the degree of which may be different for different atoms. Therefore, a rigorous analysis of the electron density in lithium clusters must be carried out with a method which in principle avoids the arbitrariness of the definition of the reference atomic densities and which provides, at the same time, a quantitative interpretation of the density distortions related to the bond formation.
A topological analysis of the charge density according to the quantum theory of atoms in molecules [18] meets all these requirements.

In this paper the results of such an analysis are presented for planar lithium clusters up to Li_6, considered in their optimal conformations obtained from all electron Hartree–Fock (HF) and Configuration Interaction (CI) calculations [5, 10, 14].

2. Computational method

Hartree-Fock and correlated wave functions have been determined for Li_2, Li_4 (D_{2h}), Li_5 (C_{2v}), planar Li_6 (D_{3h}) and pyramidal Li_6 (C_{5v}) (see Chart) using a basis set of the type [6*s*1*p*/2*s*1*p*] (basis *A*) [20] which has been proved to give reliable results for the stability of lithium clusters in comparison with the results obtained with an extended basis [10]. In order to prove that the kind and location of the critical points of the cluster electron densities do not depend to a large extent upon the choice of the basis set, three more extended basis sets have been considered: [9*s*2*p*/7*s*2*p*], [9*s*3*p*1*d*/7*s*3*p*1*d*] [5] and an uncontracted [15*s*3*p*1*d*] [21] basis denoted in the following as basis *B*, *C* and *D*, respectively.

The Li_2 molecule has been analyzed with all the basis sets, Li_4 cluster with basis *A* and *B*, while the larger clusters have been studied only with the small basis set *A*.

The correlated wave functions have been computed with the MRD CI method [22], including all the HF canonical valence and virtual orbitals in the active space while keeping the core orbitals frozen. The number of reference configurations and the selection energy threshold are such that the resulting CI wave functions are at least as accurate as those previously determined in the geometry optimization [5, 10, 14]. The details of the MRD CI treatment are reported in Table 1.

The electron densities employed in the topological analysis were obtained from CI natural orbitals and in few cases also from HF orbitals in order to elucidate the effects of the electron correlation.

The electron densities $\rho(\boldsymbol{r})$, were analyzed by means of the AIMPAC package of programs [23], according to the following steps:

(a) location, by means of a Newton-Raphson procedure, of the critical points $\boldsymbol{r}_{cp}$ of $\rho(\boldsymbol{r})$, i.e. the points were the gradient of ρ, ($\nabla\rho$) vanishes;

Table 1. Electronic properties of Li clusters computed at MRD CI level

Cluster	Basis set	Ground state	R_e (a.u.)	E_{CI} (a.u.)
Li_2	*A* [6*s*1*p*/2*s*1*p*]	$^1\Sigma_g^+$	5.28	−14.78369
Li_2	*B* [9*s*2*p*/7*s*2*p*]	$^1\Sigma_g^+$	5.10	−14.89181
Li_2 [a]	*B* [9*s*2*p*/9*s*2*p*]	$^1\Sigma_g^+$	5.10	−14.92664
Li_2	*C* [9*s*3*p*1*d*/7*s*3*p*1*d*]	$^1\Sigma_g^+$	5.10	−14.89590
Li_2	*D* [15*s*3*p*1*d*/ 15*s*3*p*1*d*]	$^1\Sigma_g^+$	5.05[b]	−14.90229
$Li_4(D_{2h})$	*A* [6*s*1*p*/2*s*1*p*]	^1A_g	5.82[b]	−29.59120
$Li_4(D_{2h})$	*B* [9*s*2*p*/7*s*2*p*]	^1A_g	5.82[e]	−29.80259
$Li_5(C_{2v})$[c]	*A* [6*s*1*p*/2*s*1*p*]	$^2A_1$	5.86	−36.99503
$Li_6(D_{3h})$[d]	*A* [6*s*1*p*/2*s*1*p*]	$^1A_1'$	6.01	−44.40715

[a] With correlation of the core orbitals
[b] Experimental distance (not optimized)
[c] $10M$, $T = 0.05 \times 10^{-6}$ hartree MRD CI treatment
[d] $10M$, $T = 0.20 \times 10^{-6}$ hartree MRD CI treatment
[e] The internal angle is 58 degrees

(b) characterization of the nature of the critical points according to the sign of their curvatures, i.e. the eigenvalues λ_i $(i=1-3)$ of the hessian matrix of ρ evaluated at $\boldsymbol{r}_{cp}$;
(c) evaluation of some properties of $\rho(\boldsymbol{r})$ at the critical points, in particular at the saddle points linking two neighbouring maxima. This latter analysis may be particularly useful since, as shown for instance in [18c], the properties of ρ computed at the minimum point of a path of maximum electron density linking two maxima (i.e. three-dimensional attractors in the vector field of the charge density gradient) is representative of the nature of the interaction involving the two attractors.

In a few selected cases the computational steps (a), (b), and (c) have been repeated also for another scalar field, that is the *Laplacian* of the charge density, defined as the trace of the Hessian matrix of ρ. In the case of Li_2 and Li_4, a numerical integration of properties (including charge, energy, volume, etc.) within quantum subspaces has been performed by employing a spherical coordinate system and standard Gaussian quadrature formulas. Because of the zero-flux surface condition - see below - the integral of $\nabla^2\rho$ within a quantum subspace should vanish and the extent to which this condition is satisfied is a test of how well the surfaces of zero-flux have been approximated. In the present study, the adopted accuracy of integration is high enough to guarantee that the value of the integrated *Laplacian* does not exceed 5×10^{-4} a.u.

A concise presentation of the theory is given in the Appendix and further details relevant to the discussion of some selected features are outlined in the text. The main parameters used in the topological analysis and their corresponding notations are collected in Table A1.

3. Charge density analysis of the Li_2 molecule

The properties of ρ at its critical points are listed in Table 2 (HF, basis sets *A*, *B*, *C*, *D*) and Table 3 (MRD CI, same basis sets). In Table 4 the data concerning the critical points of ρ and $-\nabla^2\rho$ are reported for basis *C* at various Li-Li distances.

All the results obtained on Li_2 show the rather unusual behaviour of ρ which exhibits a maximum at the Li-Li midpoint, a feature pointed out long ago by Besnainou et al. [19]. This unusual fact deserves a detailed discussion since it is of basic importance to understand the peculiar properties of the Li-Li interaction both in the Li_2 diatomic and in the Li clusters (see below).
The first general observation is that the electron density usually exhibits local maxima only at the positions of the nuclei. This fact, which is equivalent to assume that the nuclei are the only three-dimensional attractors (in the real space), allows one to define an *atom in a molecule* as the union of an *attractor* and its *basin* [24]. On this basis, a molecular system may be partitioned into a set of non overlapping basins each one containing a single nucleus. The atoms in a molecule are bounded by zero-flux surfaces in $\nabla\rho(\nabla\rho(\boldsymbol{r})\cdot\boldsymbol{n}(\boldsymbol{r})=0\ \forall\boldsymbol{r}\in S(\boldsymbol{r})$, where $\boldsymbol{n}(\boldsymbol{r})$ is the unit vector normal to the surface S at $\boldsymbol{r}$. The fulfilment of this

Table 2. ρ critical point data for Li_2 evaluated at the Hartree-Fock level with different basis sets[a]

Critical point	$R_{cp\text{-}Li}$[b]	$\lambda_{\parallel} \cdot 10^3$	$\lambda_{\perp} \cdot 10^3$	$\rho \cdot 10^2$	ρ_M/ρ_S[c]	$\nabla^2\rho \cdot 10^3$	$H \cdot 10^3$
Basis set *A*							
(3, −3)	2.679	−3.78	−2.87	1.17	—	−7.53	−2.39
(3, −1)	1.740	29.99	−3.48	1.02	1.14	23.02	−0.31
Basis set *B*							
(3, −3)	2.639	−2.70	−3.71	1.23	—	−10.12	−2.61
(3, −1)	1.836	13.15	−4.13	1.16	1.05	4.88	−2.22
Basis set *C*							
(3, −3)	2.637	−3.55	−3.74	1.28	—	−11.04	−2.84
(3, −1)	1.827	14.46	−4.62	1.21	1.06	5.22	−2.15
Basis set *D*							
(3, −3)	2.526	−4.45	−4.02	1.37	—	−12.48	−3.29
(3, −1)	1.785	16.80	−5.14	1.29	1.06	6.51	−2.20

[a] All quantities in au
[b] Distance of the critical point from the nearest atom
[c] Ratio of the charge density values at the maximum and at the (3, −1) saddle critical point

Table 3. ρ critical point data for Li_2 evaluated at the MRD CI level with different basis sets[a]

Critical point	$R_{cp\text{-}Li}$[b]	$\lambda_{\parallel} \cdot 10^3$	$\lambda_{\perp} \cdot 10^3$	$\rho \cdot 10^2$	ρ_M/μ_S[c]	$\nabla^2\rho \cdot 10^3$	$H \cdot 10^3$	$G_{\parallel}/G_{\perp}$
Basis set *A*								
(3, −3)	2.604	−3.90	−2.36	1.07	—	−8.62	−2.31	—
(3, −1)	1.759	26.10	−2.93	0.96	1.12	20.24	−0.40	97
Basis set *B*								
(3, −3)	2.550	−2.99	−3.70	1.24	—	−10.40	−2.92	—
(3, −1)	1.862	10.87	−4.28	1.20	1.03	2.31	−2.50	46
Basis set *B*[d]								
(3, −3)	2.550	−2.99	−3.82	1.27	—	−10.65	−2.96	—
(3, −1)	1.869	10.68	−4.43	1.23	1.03	1.82	−2.58	59
Basis set *C*								
(3, −3)	2.550	−4.32	−3.74	1.35	—	−11.80	−3.43	—
(3, −1)	1.811	15.37	−4.72	1.28	1.05	5.92	−2.55	25
Basis set *D*								
(3, −3)	2.526	−4.52	−3.77	1.37	—	−12.08	−3.54	—
(3, −1)	1.784	17.03	−4.88	1.29	1.06	7.28	−2.36	25

[a] All quantites in au
[b] Distance of the critical point from the nearest atom
[c] Ratio of the charge density values at the maximum and at the (3, −1) saddle critical point
[d] Including core electrons correlation

Table 4. ρ and $-\nabla^2\rho$ critical point data for Li_2 at different Li-Li distances (CI, basis C)[a]

ρ critical points								
R	Critical point	$R_{cp\text{-}Li}$[b]	$\lambda_\parallel \cdot 10^3$	$\lambda_\perp \cdot 10^3$	$\rho \cdot 10^2$	ρ_M/ρ_S[c]	$\nabla^2\rho \cdot 10^3$	$H \cdot 10^3$
4.0	(3, −1)	2.000	0.63	−0.47	1.71	—	−8.77	−5.75
4.5	(3, −3)	2.250	−5.88	−4.24	1.57	1.02	−14.35	−4.87
	(3, −1)	1.787	14.42	−5.56	1.54	—	−3.30	−3.81
5.0	(3, −3)	2.500	−4.76	−3.84	1.39	1.05	−12.43	−3.66
	(3, −1)	1.803	15.74	−4.91	1.32	—	5.92	−2.71
5.5	(3, −3)	2.750	−2.64	−3.31	1.19	1.07	−9.26	−2.62
	(3, −1)	1.852	13.01	−3.94	1.11	—	5.12	−2.04
6.0	(3, −3)	3.000	−1.02	−2.74	1.00	1.06	−6.49	−1.84
	(3, −1)	1.919	9.10	−3.02	0.94	—	3.07	−1.64

$-\nabla^2\rho$ critical points						
R	Critical point	$R_{cp\text{-}Li}$[b]	$\mu_\parallel$[d] $\cdot 10^2$	$\mu_\perp$[d] $\cdot 10^2$	$\rho \cdot 10^2$	$\nabla^2\rho \cdot 10^3$
4.0	(3, +1)	2.000	−3.60	2.34	1.71	−8.77
5.1[e]	(3, −3)	2.550	−2.05	−0.62	1.35	−11.80
6.0	(3, −1)	3.000	0.38	−0.41	1.00	−6.49
	(3, −3)	2.548	−10.08	−0.37	0.99	−6.71

[a] All quantities in au
[b] Distance of the critical point from the nearest atom
[c] Ratio of the charge density values at the maximum and at the (3, −1) saddle critical point
[d] Eigenvalues of the Hessian matrix of $-\nabla^2\rho$, evaluated at the critical point
[e] Equilibrium distance

basic condition allows to treat atoms in a molecular system as quantum mechanical subsystems for which physical observables and their expectation values are well defined: every molecular property (including energy, for instance) can be decomposed in *atomic* additive contributions [18].

Experience has shown that the majority of molecular systems conform to the above mentioned observation [18]. However, a few examples of molecules characterized by an additional maximum of ρ at positions other than nuclei have been reported by Bader et al. [18b]. The homonuclear diatomic molecules Li_2 ($X\ ^1\Sigma_g^+$), C_2 ($X\ ^1\Sigma_g^+$), Li_2^+ ($X\ ^2\Sigma_g^+$), Be_2^+ ($X\ ^2\Sigma_u^+, ^2\Pi_u$), C_2^+ ($^2\Pi_u$) exhibit a (3, −3) critical point, rather than a (3, −1) critical point (see Appendix) at the bond mid-point [18b]. These few exceptions have been found out of a study on a total of near Hartree-Fock charge densities for about 180 diatomic A_2, AB and AH molecules. In addition, until the observations reported in this paper, no non-nuclear maxima had been found in the charge distributions of the very large number of polyatomic molecules studied since the above examples were reported. The occurence of a maximum at the bond mid-point cannot be ascribed to limitations in the adopted basis set, since the charge densities of the above systems were obtained from SCF wavefunctions near to the Hartree-Fock limit, expanded in a large basis of Slater orbitals with optimized exponents. The results for Li_2 (see Table 2) confirm the occurence of a maximum of ρ at the Li-Li midpoint, a result which seems

to be substantially independent from the adopted basis set (*A*, *B*, *C*, or *D*). Since it is well known that in the case of HF wavefunctions the value of ρ in internuclear regions is overestimated with respect to the values obtained from correlated wavefunctions, it has been supposed [18b] that the small local maximum in ρ could be easily converted into a $(3, -1)$ critical point by electron correlation effects. However, the results obtained from our correlated wavefunctions for Li_2 (see Table 3) do not confirm such an expectation. In fact, the valence electron correlation, though decreasing the value of the equilibrium distance, r_e, has no significant effect on the qualitative topological features of the charge distribution. The extension of the correlation treatment to the core electrons (for basis set *B*), increases the charge density in the bonding region by a very small extent. This allows one to conclude that Li_2 ($X\ ^1\Sigma_g^+$) is characterized by an additional maximum of the charge density at a position different from the nuclear ones (Figs. 1 and 2) [25].

The general features of ρ are not modified when components of high angular symmetry are included in the basis (Basis *C*) or when a nominal basis *s* (giving an energy for Li(^2S) extremely close to the HF limit) is adopted in a fully uncontracted form in the SCF and CI calculations, thus allowing a great variational flexibility.

In Li_2 we note (Figs. 1 and 2) that the maximum (M) at the Li–Li midpoint and the two intervening saddle points (S) are well separated as indicated by both the ratio of their charge density values (ρ_M/ρ_S) and their relative distances (compare $R_{cp\text{-}Li}$ values of Table 3). For instance, ρ_M exceeds the density value at the two saddle point located 0.688 a.u. on either side of the maximum by about 5% (CI, basis set *C*). It must be recognized, however, that the absolute value of the charge density at the bond critical points (BCP) of Li_2 are exceedingly small, being for instance, 20–30 times smaller than the corresponding values computed for C–C or C–H bonds [26]. As anticipated, the accumulation of the bonding charge which is a characteristic of the HF wavefunction, is reduced by the electron correlation, which accordingly decreases the ρ_M/ρ_S ratio. However, the effect induced by the electron correlation is by far inferior to that caused by the inclusion of polarization functions. For Basis *A*, the ρ_M/ρ_S value is 1.14 and 1.12 for HF and CI wavefunction, respectively, while the corresponding values are 1.06 and 1.05 for basis set *C*.

Surprisingly, the largest curvature of the charge density at the maximum position is along the internuclear axis ($\lambda_\parallel$) and the saddle point exhibits a positive $\lambda_\parallel$ curvature which is notably higher than $\lambda_\perp$, even if both curvatures are very small in absolute value.

The presence of a maximum at the bond midpoint appears to cause some difficulties in the interpretation of the Li–Li interaction. This difficulty disappears however, when it is realized that the two Li atoms are not bonded one to another, but rather both are bonded to the central non-nuclear maximum in ρ which behaves as a pseudo atom. The properties of the two $(3, -1)$ BCP's thus characterize the nature of the bonding of each Li atom with the non-nuclear attractor.

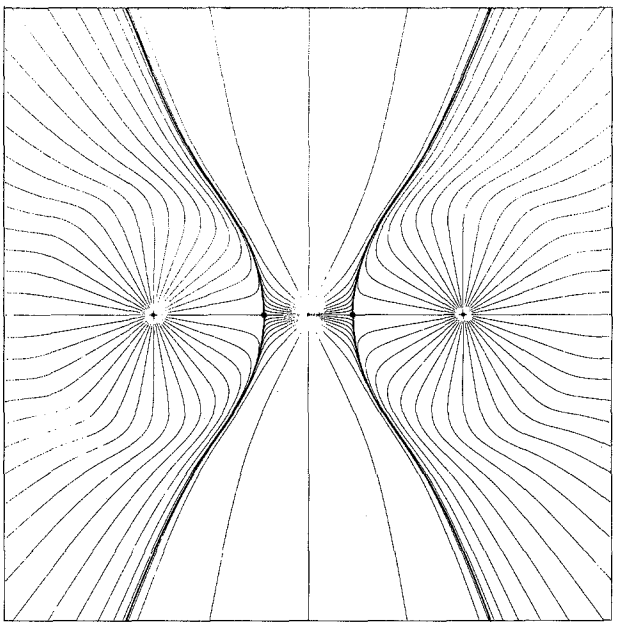

Fig. 1. Display of the gradient paths traced out by the vectors $\nabla\rho$ in a plane containing the nuclei in Li_2 (CI, Basis *C*, equilibrium geometry). The pair of trajectories which originate at the (3, −1) BCP (denoted by a *dot*) and which terminate at the neighboring attractors define a bond path, i.e. the line of maximum charge density linking the two attractors. The unique pair of trajectories which terminate at the BCP and which mark the intersection of the interbasin surfaces with the plane of the map are indicated by *heavy lines*. These latter make clear the partitioning of the molecule space into three disjoint subspaces. Two basins have a Li nucleus as a (3, −3) attractor, while in the central-one the Li-Li midpoint acts as an "anomalous" three-dimensional attractor. This is a non-nuclear subspace (see text)

At the (3, −1) BCP the Laplacian is positive, due to the dominance of the $\lambda_\parallel$ curvature of ρ, the $|\lambda_\perp|/\lambda_\parallel$ ratio is much smaller than one (0.31, CI, Basis *C*), and the $G_\parallel/G_\perp$ ratio, 25.0, is by far higher than one. These values are typical of a "closed shell" interaction which is characterized by a dominant contribution of the kinetic energy in the interaction region while the dominant potential energy contributions are separated and localized within the boundaries of the two interacting subspaces.

On the other hand, the central subspace (Fig. 2b) has a wide region characterized by a negative Laplacian (which obviously integrates to zero over the whole subspace, due to the zero-flux surface condition on $\nabla\rho$), thereby indicating a concentration of charge and a dominance of the stabilizing potential energy contribution in the Li-Li internuclear region.

These seemingly contrasting observations about the Li-Li interaction can be reconciliated if one simply realizes that its very mechanism is to create the anomalous central subspace. As a consequence, the properties at (3, −1) critical point are no longer directly related to the nature of Li-Li interaction.

It should be emphasized that Li ^2S has its Laplacian maximum in the VSCC

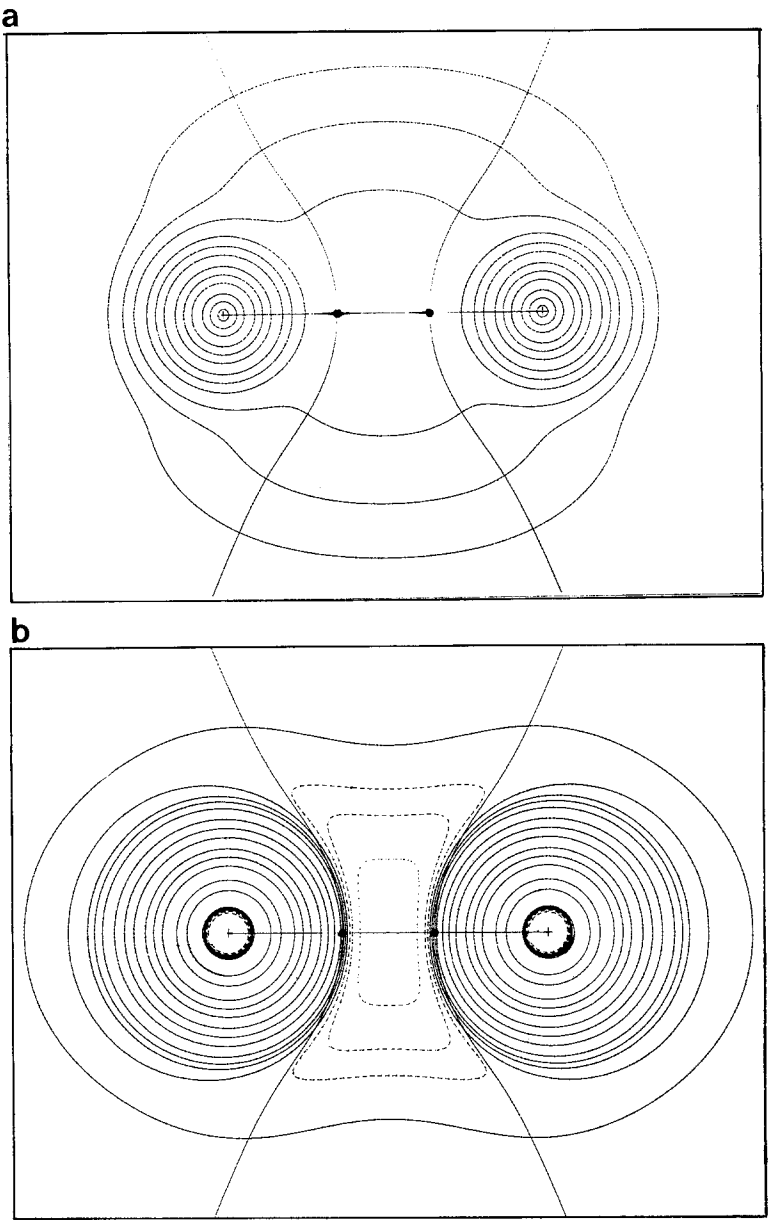

Fig. 2a, b. Li_2, CI, basis set *C*, equilibrium geometry. **a** Contour plot of $\rho(\boldsymbol{r})$ in a plane containing the nuclei. The values of the contours increase from the outermost one inwards in steps of 2×10^n, 4×10^n and 8×10^n with n beginning at -3 and increasing in step of unity (the same contour were used for the other maps of ρ). The pair of trajectories which originate (bond paths) or which terminate at the BCP (denoted by *dots*) are superposed on the contour map. **b** Contour plot of $\nabla^2\rho(\boldsymbol{r})$ in a plane containing the nuclei. *Dashed contours* denote negative, *solid contours* positive values of $\nabla^2\rho$ (regions of charge concentration and charge depletion, respectively). The contour values in au are $+/-0.002$, $+/-0.004$, $+/-0.008$ increasing in powers of 10 to $+/-8.0$. The outermost contour is 0.002 au (this set of contours is used throughout the paper for $\nabla^2\rho$). The local charge concentration (3, -3) critical point in $-\nabla^2\rho$ is located at the Li-Li midpoint and coincide with the local maximum in ρ. Note the characteristic wide region of charge concentration ($\nabla^2\rho<0$) in the internuclear zone of the non-nuclear subspace

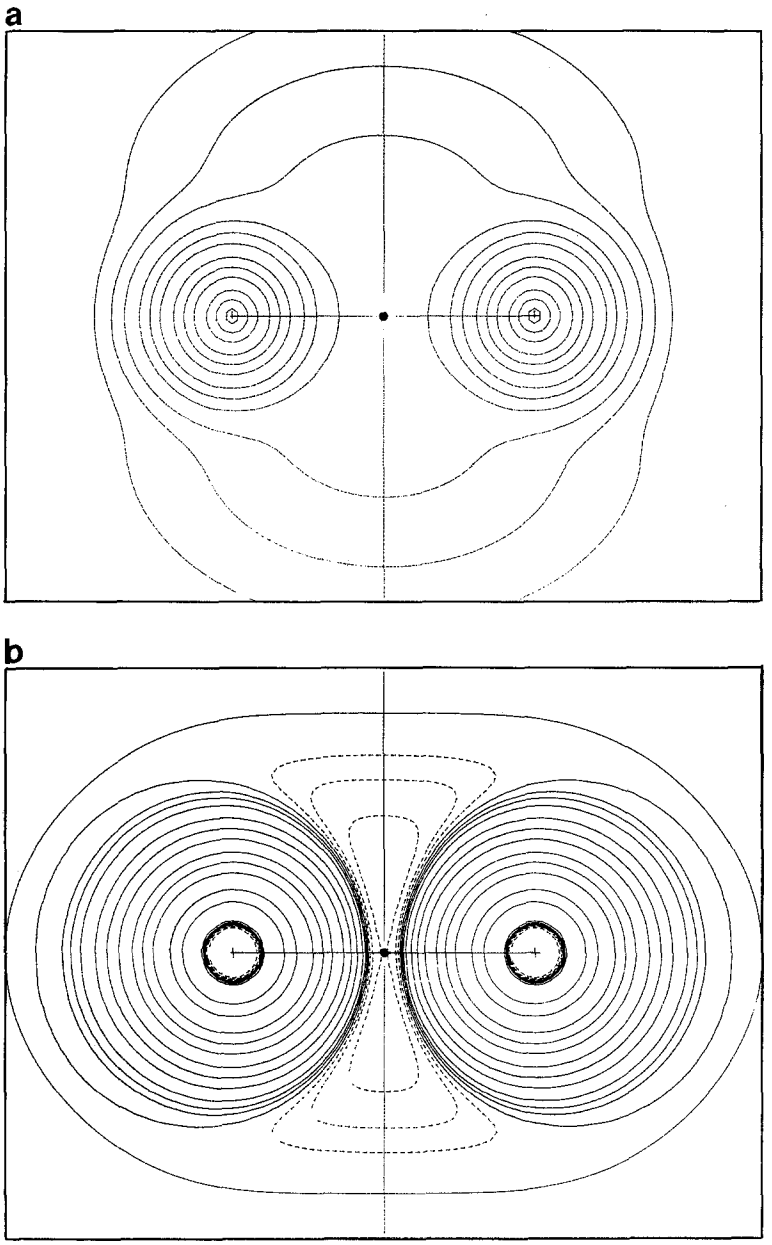

Fig. 3a, b. Li_2, CI, Basis *C*, $R_{Li-Li} = 4$ au. **a** Contour plot of $\rho(\boldsymbol{r})$ in a plane containing the nuclei. The (3, −3) critical point at the internuclear axis midpoint (Fig. 1 and 2a) disappeared and the usual (3, −1) saddle point is formed (denoted by a *dot*). Therefore, the molecular space is divided in two quantum subspaces only. **b** Contour plot of $\nabla^2\rho(\boldsymbol{r})$ in a plane containing the nuclei. Because of the compenetration of the valence shell charge concentration of the two Li atoms, a toroidal region of maximum charge concentration is created around the Li–Li axis. The maximum in $-\nabla^2\rho$ at the Li–Li midpoint for the equilibrium configuration (Fig. 2b) is accordingly converted in a (3, +1) critical point. This latter coincides in location with the (3, −1) ρ critical point (denoted by a *dot*)

(Valence Shell Charge Concentration) at 2.488 a.u. (Basis *B*), a distance which closely resembles the r_e of Li_2 (2.550 a.u.) and which is very large because of the presence of just one electron in the valence shell. Though there is neither a physical nor a mathematical direct relation between the spatial coincidence of maxima in ρ and $-\nabla^2\rho$ [28], the crude observation remains that a close similarity between r_e and the radius of the sphere in which the valence charge density is maximally concentrated, complies with the creation of an anomalous mid-point maximum in ρ.

By shortening the Li-Li distance to 4 au, the VSCC of the two Li atoms overlap and a toroidal region of maximum charge concentration is created around the Li-Li axis (Table 4 critical point in $-\nabla^2\rho$ and Fig. 3b) and the usual BCP appears at the Li-Li midpoint (CI, Basis *C*, see Table 4 and Fig. 3a).

Since the central non-nuclear subspace is a quantum subspace, it can be characterized also in terms of its average properties. As it is shown in Table 5, the contribution to the total energy of non-nuclear subspace amounts to 0.1149 a.u. only (as an obvious consequence of the lack of a nucleus) but its total electronic charge is higher than one. The "free electron" nature of this charge is clearly

Table 5. Atomic properties (au) of quantum Ω subspaces of Li_2 evaluated at the MRD CI level with basis *A*, *B*, and *C*

Ω	$-E(\Omega)$[a]	$N(\Omega)$[b]	$V(\Omega)$[c]	$V/e(\Omega)$[d]	$\Delta r(\Omega)$[e]
Basis set *A*					
Li	7.3417	2.388	59.6	25.0	−0.22
Ω^f_{nn}	0.1003	1.194	180.9	147.9	—
$Li+\Omega_{nn}$	7.4420	3.612	240.5	66.6	—
Basis set *B*					
Li	7.4114	2.567	85.1	33.2	−0.15
Ω^f_{nn}	0.0690	0.866	122.4	141.3	—
$Li+\Omega_{nn}$	7.4804	3.433	207.5	60.4	—
Basis set *C*					
Li	7.3971	2.426	64.8	26.7	−0.15
Ω^f_{nn}	0.1017	1.148	156.1	136.0	—
$Li+\Omega_{nn}$	7.4988	3.574	220.9	61.8	—

[a] The subspace energy $E(\Omega)$ is obtained by integration of the kinetic energy density (see Appendix) over the basin of the subspace ($E(\Omega) = -T(\Omega)$, where $T(\Omega)$ is the subspace kinetic energy). Due to the fact that the virial theorem is not exactly satisfied at the employed level of theory, each integrated kinetic energy was multiplied by the factor $(\gamma-1)$, γ being the computed virial ratio, in order to obtain a set of atomic energies that correctly sum to the total energy of the molecule

[b] Total electronic charge of Ω, $N(\Omega) = -\int_\Omega \rho\, d\tau$

[c] The subspace volumes $V(\Omega)$ were computed as the region of space enclosed by the intersection of the subspace surface of zero-flux and the 0.002 au envelope of the charge density

[d] $V/e(\Omega)$ is the mean value for electron in Ω, defined as $V(\Omega)/N(\Omega)$

[e] $\Delta r(\Omega)$ is the displacement of the centroid of negative charge of Ω from the position of its (3, −3) attractor. A minus sign indicates that the centroid is displaced in the opposite direction of the line joining the two Li nuclei

[f] Ω_{nn} is the subspace associated with the non-nuclear attractor at the midpoint of the internuclear axis

indicated by the comparison of the mean volume per electron values (V/e) computed for the Li basin (26.71 a.u.) and the central non-nuclear subspace (135.98 a.u.).

4. Analysis of the charge density in Li_4, Li_5 and Li_6

4.1. Li_4 cluster

The properties of ρ at its critical points are listed in Table 6. In Fig. 4a,b the contour plots of $\rho(\boldsymbol{r})$ and $\nabla^2\rho(\boldsymbol{r})$ in the molecular plane are reported (xy, see chart). In the same figures the $\nabla\rho(\boldsymbol{r})$ trajectories, associated with the $(3,-1)$ critical points, are superimposed on the contour maps, thereby defining the boundaries of the quantum subspaces of Li_4 and its associated molecular graph (see Appendix).

As shown in Fig. 4 the molecular space of Li_4 is partitioned in six basins: four contain a nucleus while the remaining two do not. These latter non-nuclear subspaces share their interbasin surfaces with each other and with the three nearest neighboring atoms. The two $(3,-3)$ non-nuclear attractors are individually bonded to three Li nuclei and the two triplets of nuclei are linked only indirectly through the bond path joining the two attractors.

The above analysis leads to the very important conclusion that the Li atoms are not bonded directly to one another. There are no Li–Li bonds. The bond path connecting the two non-nuclear attractors and the two bond paths connecting the attractors to the same Li nucleus form a three-membered ring enclosing a

Table 6. ρ critical point data for $Li_4(D_{2h})$, evaluated at the MRD CI level with basis A and B[a]

Critical point $\lvert m\rvert$[b]	$R_{cp\text{-}Li(n)}$[c]	$\lambda_1\cdot10^3$	$\lambda_2\cdot10^3$	$\lambda_3\cdot10^3$	$\rho\cdot10^2$	$\nabla^2\rho\cdot10^3$	$H\cdot10^3$	ε
Basis set A								
$(3,-1)\lvert1\rvert$	2.551 (1)	−3.14	−1.92	2.48	0.81	−2.58	−1.56	0.63
$(3,-3)\lvert2\rvert$	2.618 (3)	−3.15	−3.04	−1.28	1.15	−7.47	−2.17	—
	3.653 (1)							
$(3,-1)\lvert3\rvert$	1.745 (3)	−3.36	−1.96	28.30	1.02	22.98	−0.32	0.71
$(3,-1)\lvert4\rvert$	1.774 (1)	−3.68	−2.08	27.80	0.84	22.04	0.28	0.77
$(3,+1)\lvert5\rvert$	1.838 (1)	−2.46	1.80	1.58	0.75	15.17	−0.23	—
Basis set B								
$(3,-1)\lvert1\rvert$	2.551 (1)	−3.14	−1.94	1.27	0.92	−3.80	−1.96	0.62
$(3,-3)\lvert2\rvert$	2.287 (3)	−3.11	−2.56	−1.23	1.13	−6.89	−2.26	—
	3.896 (1)							
$(3,-1)\lvert3\rvert$	1.914 (3)	−3.30	−1.87	6.21	1.12	1.05	−2.26	0.77
$(3,-1)\lvert4\rvert$	1.917 (1)	−4.11	−2.00	9.67	0.98	3.57	−1.82	1.06
$(3,+1)\lvert5\rvert$	1.968 (1)	−3.40	1.26	6.32	0.90	4.18	−1.71	—

[a] All quantities in au

[b] The number in bracket is the critical point identification number reported in Fig. 4a

[c] The atom to critical point distance refers to the lithium atom whose identification number is reported in parentheses (see Fig. 4a)

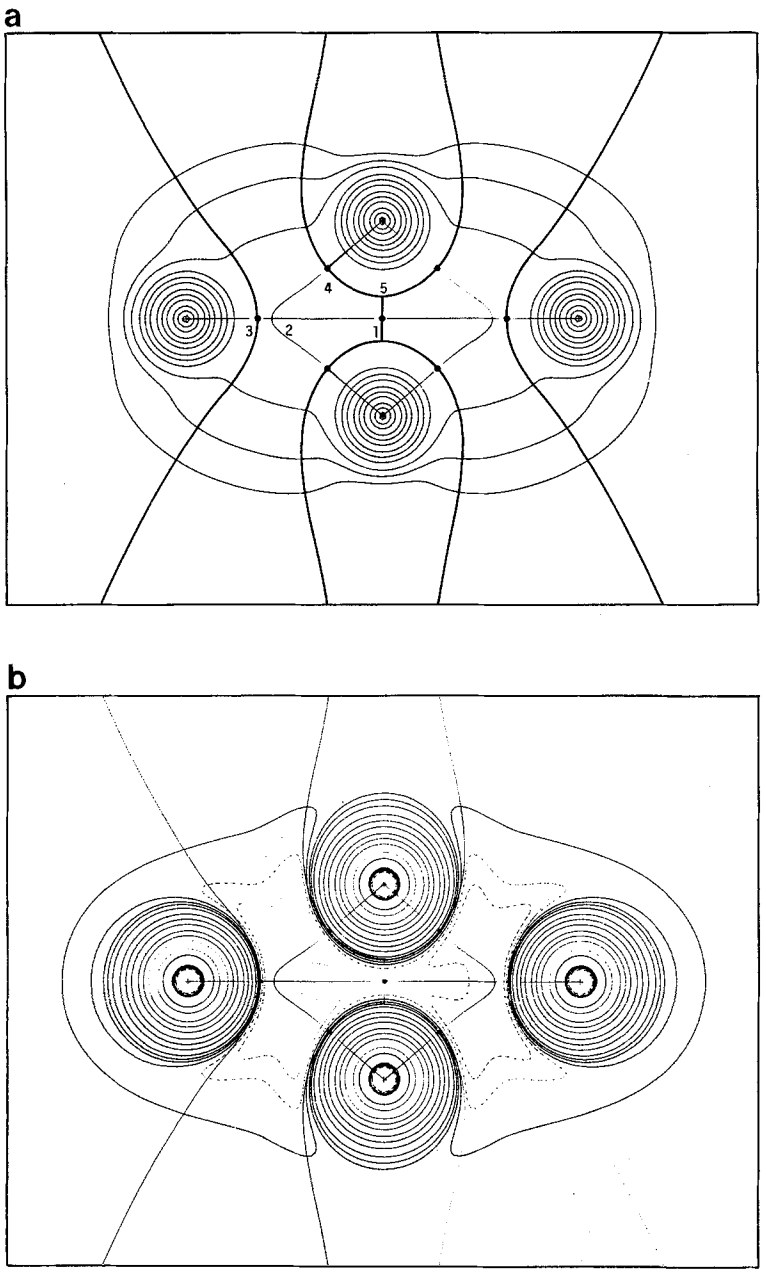

Fig. 4a, b. $Li_4(D_{2h})$, CI, Basis *B*. **a** Contour plot of $\rho(\boldsymbol{r})$ in the molecular plane. The pair of overlayed $\nabla\rho$ trajectories which originate at the BCPs (denoted by *dots* and by the identification number reported in Table 6) define the molecular graph for Li_4. Accordingly, Li atoms are not linked each other but are bonded only to the non-nuclear attractors (labelled as 2). The $\nabla\rho$ trajectories which terminate at the BCPs are indicated by *heavy lines* and partition the molecular space in six quantum subspaces, two of which are non-nuclear subspaces. **b** Contour plots of $\nabla^2\rho(\boldsymbol{r})$. *Dashed contours* denote negative, *solid contours* positive values of $\nabla^2\rho(\boldsymbol{r})$, respectively

surface within which the charge density attains a minimum value at the (3, +1) critical point (labelled as 5 in Fig. 4a). Due to the symmetry of the system there are two of such rings, sharing a common side.

The different bond critical points (see Table 6) yield a hierarchy:

(i) BCPs between a non-nuclear attractor and a lithium center which has two nearest neighbors (hereafter denoted as Li(2*nn*) atom. Each Li(2*nn*) atom has just one BCP, labelled 3 in Fig. 6.
(ii) BCPs between a non-nuclear attractor and a Li atom which has three nearest neighbors (hereafter denoted as Li(3*nn*)). Each Li(3*nn*) has two BCPs, the one labelled as 4 in Fig. 6 and its symmetric one.
(iii) BCPs between the non-nuclear attractors.

Each non-nuclear attractor has in overall four BCPs; one of the type non-nuclear - non-nuclear (BCP 1 in Fig. 6), one of type non-nuclear - Li(2*nn*), and two of type non-nuclear - Li(3*nn*).

The charge density computed at the BCPs 3, 4, and 1 of Fig. 6 amounts to 1.02, 0.84 and 0.81 au for Basis *A*, and 1.12, 0.98 and 0.92 au for Basis *B*, respectively. These values agree with the above reported ordering scale. It should be noted that the charge density at BCP 1 is a local maximum along the *y* direction, that is the line joining the two Li(3*nn*) atoms. The situation is in some respect similar to that occuring in the Li_2 molecule. However, the two Li(3*nn*) atoms are no

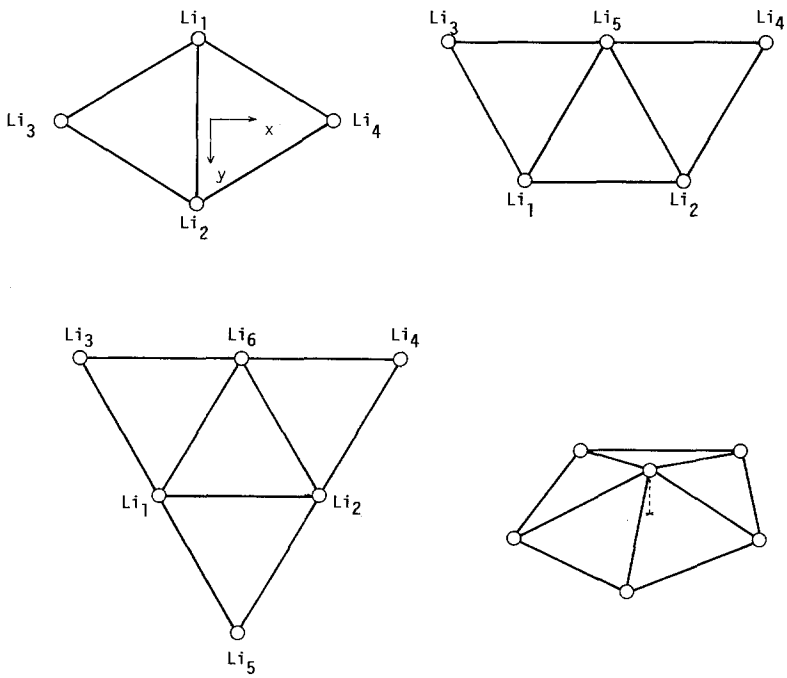

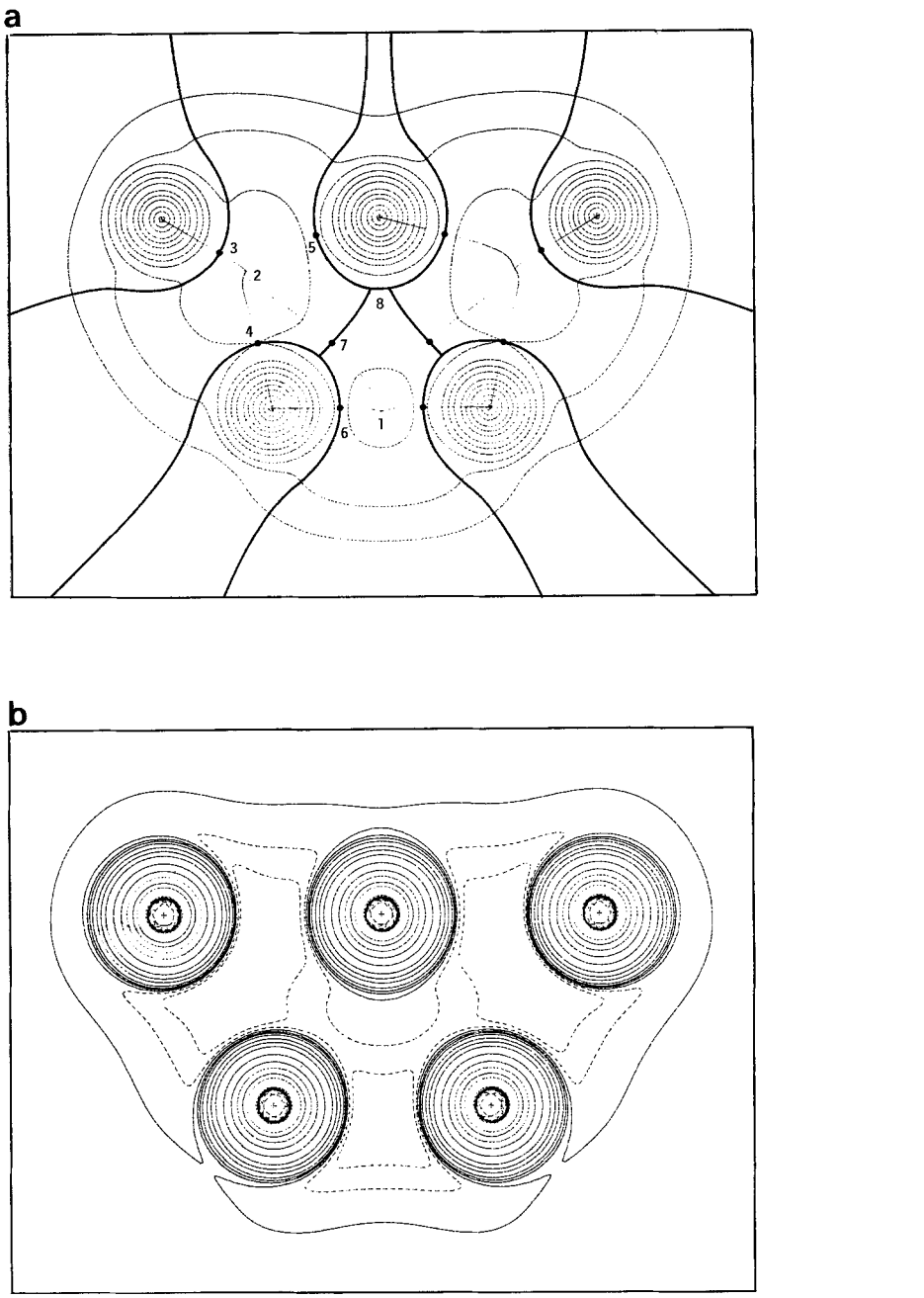

Fig. 5a, b. Li_5 (C_{2v}), CI, Basis *A*. **a** Contour plot of $\rho(\boldsymbol{r})$ in the molecular plane. The BCPs are denoted by dots and by the identification number of Table 8. Borders of the quantum subspaces are indicated by *heavy lines*. There are three non-nuclear subspaces, whose attractors are the critical points 1 and 2. **b** Contour plots of $\nabla^2\rho(\boldsymbol{r})$. *Dashed contours* denote negative, *solid contours* positive values of $\nabla^2\rho(\boldsymbol{r})$, respectively

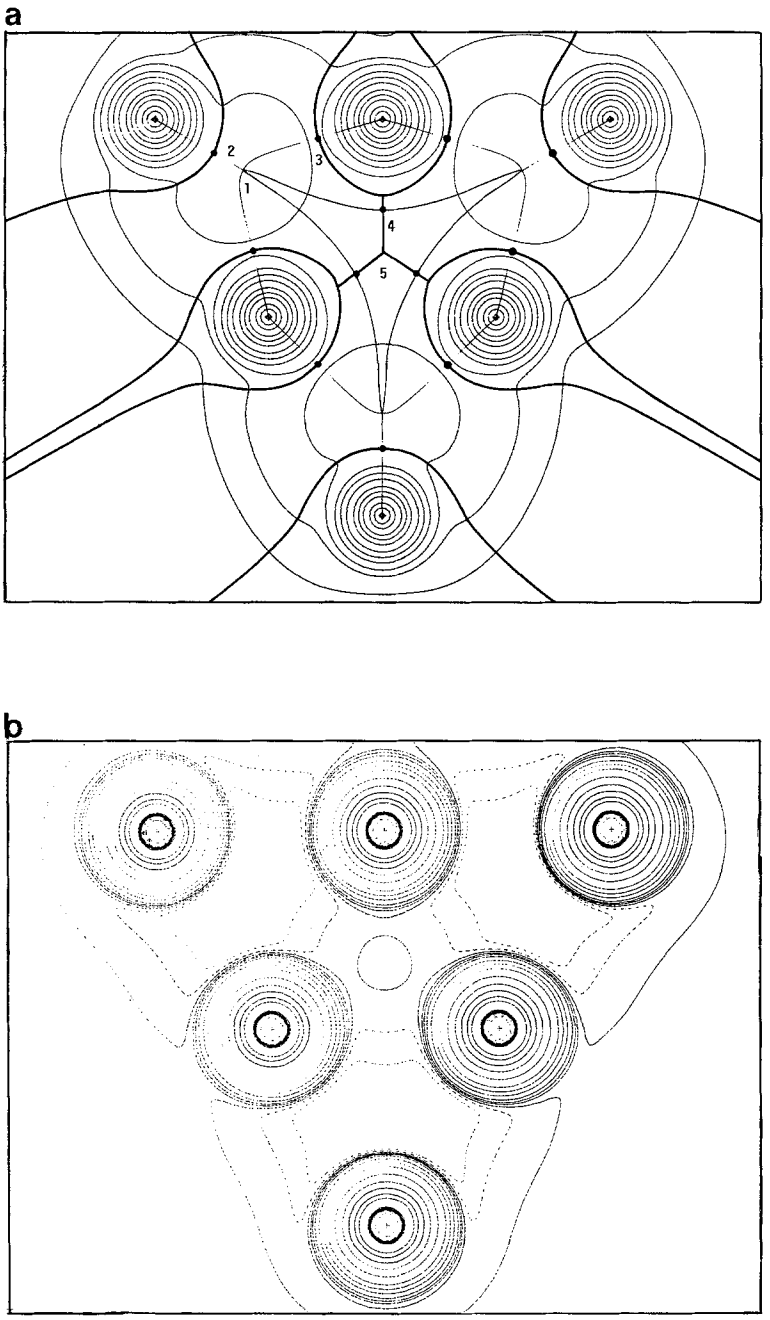

Fig. 6a, b. Li_6 (D_{3h}), CI, Basis *A*. **a** Contour plot of $\rho(\boldsymbol{r})$ in the molecular plane. The BCPs are denoted by *dots* and by the identification number of Table 9. Borders of quantum subspaces are indicated by *heavy lines*. The three non-nuclear attractors (labelled as 1) are all linked to each other. **b** Contour plots of $\nabla^2\rho(\boldsymbol{r})$. *Dashed contours* denote negative, *solid contours* positive values of $\nabla^2\rho(\boldsymbol{r})$, respectively

Table 7. Atomic properties (au) of quantum Ω subspaces of Li_4 evaluated at the MRD CI level with basis *A* and *B*

Ω	$-E(\Omega)$[a]	$N(\Omega)$[b]	$V(\Omega)$[c]	$V/e(\Omega)$[d]	$\Delta r(\Omega)$[e]
Basis set *A*					
Li_1	7.2858	2.112	31.4	14.9	−0.28
Li_3	7.3673	2.432	71.1	29.2	−0.01
Ω^f_{nn}	0.1425	1.456	216.3	148.6	—
Basis set *B*					
Li_1	7.3697	2.229	48.6	21.8	−0.21
Li_3	7.4315	2.634	96.6	36.7	−0.03
Ω^f_{nn}	0.1001	1.137	168.7	148.3	—

[a–d] See the corresponding footnotes in Table 5

[e] A minus sign indicates that the centroid of negative charge is displaced in the opposite direction with respect to the equivalent Li nuclei

[f] Ω_{nn} is one of the two non-nuclear subspaces

longer indirectly linked through a central basin, since they have increased their "valence" to two in order to be able to link the two non-nuclear attractors. The mechanism which splits each of the bond paths in Li_2 into two distinct bond paths forming an angle of 95°, results in the formation of a ring critical point (denoted as 5 in Fig. 4a).

The quantum theory of atoms in molecule can determine to what extent the atomic properties - including net charge, atomic dipoles, energies, volumes - are transferable between molecules [29]. In the present context, the Li(3*nn*) and Li(2*nn*) atoms are expected to exhibit quite different atomic properties, due to the noteworthy difference in their charge distribution. As shown in Table 7, Li(2*nn*) has 0.405 electrons more than Li(3*nn*), a basin volume twice larger than that of Li(3*nn*), and a V/e value 1.7 times larger. Li(2*nn*) is also more stable than Li(3*nn*) by 38.7 kcal/mol (Basis *B*) as a consequence of its greater electronic charge.

The comparison with the corresponding properties (Table 5) indicates a close similarity of the Li(2*nn*) atoms of Li_4 with those of the Li dimer. The Li(3*nn*) atoms increase their "valence" at the expense of their energy.

These considerations on the charge density topology can also rationalize the important differences found in the Mulliken population data. Li(3*nn*) atoms have a total *s* and *p* occupancy equal to 2.5 and 0.3 electrons, respectively, while the corresponding values for Li(2*nn*) atoms are 3.1 and 0.06 (Basis *A*). Furthermore the p_x population on Li(3*nn*) is about 6 times larger than the p_y occupancy. A population analysis based on Lowdin partitioning, gives results which further confirm the differences between Li(2*nn*) and Li(3*nn*) atoms.

These results shed light on the mechanism which makes the *p* polarization functions so important for the description of stable Li clusters. In this respect Li(2*nn*) and Li(3*nn*) atoms turn out to play a quite different role just because of their different degree of *sp* hybridization. Furthermore, this fact indicates that a conventional EDM analysis of the electron density redistribution in Li_4 caused by the bond formation is, to a large extent, arbitrary, due to the basic difficulty to uniquely define a reference electron density for isolated atoms.

As shown in Table 7, each non-nuclear subspace created by the mutual approach of the four Li atoms, encloses a charge of 1.456 e (Basis A) and has a V/e value of 148.6 a.u. Overall the two non-nuclear subspaces possess a charge and a volume that amount to 24% and 68% of the total molecular electronic charge and volume. These values are slightly higher than those computed for Li_2 (Basis A): 20% and 61%, respectively.

The comparison of the results so far described for Li_2 and Li_4 allow one to anticipate the very important conclusion that, as the cluster grows, the non-nuclear subspaces not only preserve but even increase their number, extension and charge as well.

The ρ values at BCPs (Table 6), though differentiated by their topological nature, indicate that the overall charge density distribution in the central region of the cluster is nearly flat.

A few comments are in order as for the different descriptions given by different basis sets. The comparison of the values of Table 3 shows some discrepancies between results obtained with basis A and B. While basis B gives a general lowering of charge density with respect to Li_2, the basis A indicates an increase of ρ value at the non-nuclear maxima and saddle points of type i) [30]. However, the important observation is that both basis sets describe the electronic charge in the central region of Li_4 as spatially diffuse. In fact, the ellipticity values ε at the saddle points, with ε ranging from 0.62 to 1.06 (Basis B) and from 0.63 to 0.77 (Basis A) show a high degree of π character for non-nuclear - Li and non-nuclear - non-nuclear bonds and the direction of the eigenvectors associated with the λ_2 curvature indicate that the charge is preferentially accumulated in the molecular plane. As expected from its noteworthy *sp* hybridization the highest ellipiticity is found for the bond path associated with the Li($3nn$) atoms ($\varepsilon = 1.06$, Basis B), a value higher than that found in cyclopropane: $\varepsilon = 0.49$ [32, 33].

The preferential in-plane accumulation of charge density in the non-nuclear region of Li_4 is also clearly illustrated by the variations in the values of the components of the quadrupole moment Q_{ii}, ($i = x, y, z$) [34] for a cluster atom, say a Li($2nn$) atom, when a non-nuclear subspace is also included in the integration. The highly negative value (−2.55 au, Basis B) for the Q_{zz} component of Li($2nn$) atom, is strongly lowered ($Q_{zz} = -0.31$ au) for the combined Li($2nn$) and non-nuclear subspace and becomes even highly positive in the case of minimal basis set (4.95 a.u.).

All the BCPs but 1 - the saddle point joining the two non-nuclear attractors - exhibit a positive value of $\nabla^2\rho$ like in Li_2. The negative $\nabla^2\rho$ value at critical point 1 (-3.80×10^{-3} a.u., basis B) is clearly due to its ambivalent nature. Since BCP 1 is a maximum along the Li($3nn$)-Li($3nn$) line, its $\nabla^2\rho$ value is expected to be negative as found in Li_2. However, its absolute value is lowered with respect to the diatomic case (-10.40×10^{-3} au, basis B) because BCP 1 also connects two non-nuclear attractors.

Overall, the internuclear region associated with the innermost part of the two non-nuclear subspaces, has a negative Laplacian, as in the case of Li_2. This

Table 8. ρ critical point data for $Li_5(C_{2v})$, evaluated at the MRD CI level with basis A[a]

Critical point $\|m\|$[b]	$R_{cp\text{-}Li(n)}$[c]	$\lambda_1 \cdot 10^3$	$\lambda_2 \cdot 10^3$	$\lambda_3 \cdot 10^3$	$\rho \cdot 10^2$	$\nabla^2\rho \cdot 10^3$	$H \cdot 10^3$	ε
(3, −3) |1|	2.931 (1)	−2.49	−1.87	−1.65	0.88	−6.01	−1.74	—
(3, −3) |2|	2.632 (3)	−2.74	−2.59	−0.98	1.04	−6.31	−1.84	—
	3.733 (1)							
	3.896 (5)							
(3, −1) |3|	1.770 (3)	−3.00	−1.61	24.01	0.94	19.39	−0.32	0.86
(3, −1) |4|	1.791 (1)	−3.08	−1.81	23.93	0.80	19.04	0.15	0.70
(3, −1) |5|	1.795 (5)	−3.29	−2.02	24.95	0.74	19.64	0.38	0.63
(3, −1) |6|	1.809 (1)	−2.79	−1.74	20.04	0.77	15.51	−0.23	0.60
(3, −1) |7|	2.381 (1)	−2.35	−1.74	1.58	0.72	−2.51	−1.30	0.35
	3.574 (5)							
(3, +1) |8|	1.891 (5)	−1.87	1.26	1.26	0.55	12.04	0.14	—
	4.325 (1)							

[a] All quantities in au

[b] The number in bracket is the critical point identification number reported in Fig. 5a

[c] The atom to critical point distance refers to the lithium atom whose identification number is reported in parentheses (see Fig. 5a)

confirms that the stabilization is predominantly due to the lowering of potential energy which occurs in this region characterized by a flat and delocalized electronic distribution (Fig. 4b).

4.2. Li_5 cluster

The properties of ρ at its critical points are listed in Table 8. The contour plots of $\rho(\boldsymbol{r})$ and $\nabla^2\rho(\boldsymbol{r})$ are displayed in Fig. 5a, b, respectively. The $\nabla\rho(\boldsymbol{r})$ trajectories (overlayed on the ρ contour map) associated with the (3, −1) critical point, show that the molecular space is partitioned in eight quantum subspaces: five contain a Li nucleus, while the remaining are non-nuclear subspaces.

Non-nuclear attractors like 2 in Fig. 5a are linked to a Li(2*nn*), a Li(3*nn*), and a Li(4*nn*) atom and to the unique non-nuclear attractor labelled as 1. This latter is also bonded to two Li(3*nn*). The molecular graph of Li_5 (Fig. 5a) makes clear that Li atoms are not directly bonded among themselves, as it has been found in the case of rhombic Li_4. Similarly, the non-nuclear attractors all have a formal valence equal to four, while the Li atoms are unable to increase their valence beyond two: the valence is one for Li(2*nn*) and two for Li(3*nn*) and Li(4*nn*) atoms. In particular, since the valence of Li(4*nn*) is already saturated by the non-nuclear attractors of type 2, Li(4*nn*) cannot be bound also to the non-nuclear attractor 1, which, in fact, is located far from Li(4*nn*) and slightly displaced outwards (0.1 a.u.) with respect to the line joining the two Li (3*nn*).

It is apparent that the Li_5 cluster would need an additional atom in order to recover the favourable pattern for planar clusters, i.e. maxima in the interior of the triangles [35]. It should be noted also that these maxima have a higher ρ value (1.04×10^{-2} a.u.) with respect to the edge maximum (0.88×10^{-2} a.u.) because of the positive interference effect of a 3-atom instead of a 2-atom

interaction. Similar results were obtained also for Li_4 though the ρ value at the critical point 1 (Fig. 4a) is further reduced due to its ambivalent nature (see above).

The bond critical points of Li_5 can be classified on the basis of considerations similar to those commented for Li_4. For the sake of conciseness, we just note that the ρ values at the BCPs are in general smaller than the corresponding values in Li_4 and Li_2 (for example, the ρ value for Li(2*nn*) - non-nuclear BCP is 1.02×10^{-2} and 0.94×10^{-2} au for Li_4 and Li_5, respectively) and can be ordered according to the sequence Li(2*nn*) > Li(3*nn*) > Li(4*nn*) > non-nuclear. In fact, the highest value is found for Li(2*nn*) - non-nuclear BCP and the lowest one (0.72×10^{-2} a.u.) pertains to the non-nuclear - non-nuclear BCP (labelled as 7 in Fig. 5a).

Also the different saddle points of Li(3*nn*), which connect two different types of non-nuclear attractors, are well characterized and the different values of charge density, ellipticity and energy density of BCPs 4 and 6 can be rationalized by considering that the non-nuclear attractor 1 is an edge maximum.

The ellipticity values at the saddle points and the out of plane direction of the eigenvector associated with the λ_1 curvature, indicate a preferential accumulation of charge in the molecular plane, as for Li_4. The only exception is BCP 7 which has a low value of ellipticity and a preferential out of plane charge accumulation. BCP 7 is located between two regions of in-plane charge accumulation and its apparently anomalous properties (Table 8) confirm the regional localization (i.e. edge, triangle) of the in-plane charge accumulation.

Furthermore, the λ_3 curvature at BCP 7 is exceedingly small (typically one tenth of the corresponding value for the other BCPs) thus indicating a general flatness in the inner region of the cluster. It is precisely the low value of λ_3 which makes negative the Laplacian at BCP 7, in agreement with both its location in the region in which the potential energy dominates (Fig. 5b) and with its particular nature; a BCP generated by the interaction of two non-nuclear attractors.

Table 9. ρ critical point data for $Li_6(D_{3h})$, evaluated at the MRD CI level with basis A[a]

Critical point $\|m\|$ [b]	$R_{cp\text{-}Li(n)}$ [c]	$\lambda_1\cdot10^3$	$\lambda_2\cdot10^3$	$\lambda_3\cdot10^3$	$\rho\cdot10^2$	$\nabla^2\rho\cdot10^3$	$H\cdot10^3$	ε
(3, −3) |1|	2.692 (3) 3.921 (1, 6)	−2.83	−2.45	−1.16	1.06	−6.44	−1.78	—
(3, −1) |2|	1.765 (3)	−3.07	−1.86	25.14	0.94	20.22	−0.23	0.65
(3, −1) |3|[g]	1.793 (1)	−3.27	−2.38	25.03	0.75	19.38	0.37	0.38
(3, −1) |4|	2.368 (6) 4.140 (1)	−1.13	−0.95	1.82	0.50	−0.27	−0.73	0.18
(3, +1) |5|	3.476 (1, 2, 6)	−1.20	0.76	0.77	0.48	0.33	0.53	—

[a] All quantities in au

[b] The number in bracket is the critical point identification number reported in Fig. 6a

[c] The atom to critical point distance refers to the lithium atom whose identification number is reported in parentheses (see Fig. 6a)

4.3. Li_6 cluster

The properties of ρ at its critical points are listed in Table 9. The contour plots of $\rho(\boldsymbol{r})$ and $\nabla^2\rho(\boldsymbol{r})$ are displayed in Fig. 6a and 6b, respectively. Li_6 consists of nine quantum subspaces; six of them contain a nucleus, while the remaining three are non-nuclear subspaces. Because of the symmetry of the system, the non-nuclear attractors are all equivalent, linked to each other and exhibiting a "valence" increased to five.

The topology of the charge distribution indicates the existence of four three-membered rings. The central one, which is delimited by bond paths strongly curved inwards, is formed only by the non-nuclear attractors, while one vertex of the other equivalent three rings is a Li(4*nn*) atom.

The charge density properties at BCP labelled as 2 and 3 in Fig. 6a, closely resemble the corresponding BCP values for Li(2*nn*) and Li(4*nn*) in Li_5 cluster, aside lower ellipticity values. This and the corresponding similarity found for the non-nuclear maxima values, strongly suggests that the BCP properties are nearly transferable from cluster to cluster.

The topology of Li_6 confirms that lithium planar clusters prefer a structure made up by Li triplets of atoms which are only indirectly linked through non-nuclear maxima. Each triplet is composed of one Li(2*nn*) and two Li(4*nn*) atoms. As in the case of Li_5, a maximum can not be found in the innermost triangle because of the incapability of Li(4*nn*) atoms to increase their "valence" beyond two. On the contrary, the non-nuclear attractors are more flexible in expanding their "valence", due to their not atomic-like nature.

The separate localization of the charge accumulation in the outermost triangles is further confirmed by the positive value of the Laplacian in the internal triangle.

Finally, it is interesting to note that as the planar clusters grow, the nearest neighbor distances increase (Table 1) and so do, on average, the Li-BCP separation. However, the BCP shift is comparatively much smaller. In fact, the $R_{\text{Li-BCP}}/r_e$ ratio is 0.34 for Li_2 and ranges from 0.30–0.31 for Li_5 to 0.29–0.30 for Li_6. These data suggest that the cluster increases its nearest neighbor distance value, with respect to Li_2, in order to maximize the spatial extension of non-nuclear subspaces. The integration data reported for Li_4 further confirm this view.

5. Conclusions

It has been demonstrated [18] that subspaces of a molecular system are quantum mechanically well-defined provided they are bounded by zero-flux surfaces in $\nabla\rho$ at each point of the surface. However, *there is no a priori indication* that these subspaces should be associated with an atomic region. Nonetheless, the observation that the number of subspaces in a molecule usually equals the number of its constituting atoms and that each subspace contains just one atomic nucleus, has compelled to the identification of these subspaces with the atoms in a molecule [18].

The results obtained here clearly indicate that in unusual chemical entities like lithium clusters, subspaces do exist which do not enclose a nucleus. Nevertheless, they possess a point in their domain which is a sink for the gradient vector field of their associated basin. This is a striking indication of the peculiar chemical nature of Li clusters and, at the same time, a generalization of the quantum theory of atoms in molecules to systems in which electrons partially behave as mobile metallic electrons.

By examining two-dimensional closed-packed arrays of Li atoms, Goddard and McAdon [15] point out the general result that GVB orbitals are localized at the centers of triangles (2 singly-occupied GVB orbitals, singlet paired), while surface (edge) regions have orbitals localized at bond midpoints, a description which qualitatively agrees with our results.

The advantage of the analysis carried out in the present work is to provide a quantitative estimate of the charge (and charge dependent properties) modifications accompanying the bond formation of a given cluster and the cluster growth process.

The role played by the formation of ρ maxima in triangular units in stabilizing the cluster is well documented by the computed incremental binding energy per atom for the cluster growth $Li_a \rightarrow Li_b$: $\Delta\bar{E}_{b-a} = (\bar{E}_b - \bar{E}_a)/(b-a)$, where $\bar{E}_i$ is the mean atom energy E_i/i. The relatively high $\Delta\bar{E}_{4-2}$ value, 1.88 kcal/mol, is due to the creation of two "triangular" maxima and the annihilation of two "edge" maxima. $\Delta\bar{E}_{5-4}$ is smaller than $\Delta\bar{E}_{4-2}$ (0.75 kcal/mol) because only one additional edge maximum is formed, while $\Delta\bar{E}_{6-5}$ increases to 1.38 kcal/mol because of the formation of a third triangular maximum, at the expense of an edge maximum.

The maxima located in triangles defined by the Li atoms not only are responsible for the cluster stability increasing with the nuclearity but show a high degree of transferability from cluster to cluster, also from a geometrical point of view. In particular, the non-nuclear maxima are not equidistant from the Li atoms to which they are bonded but the distances $R_{cp\text{-}Li(Xnn)}$ are nearly constant for a given X. In fact, in the series Li_n ($n = 4, 5, 6$) the $R_{cp\text{-}Li(Xnn)}$ distances vary in the ranges 2.618–2.692, 3.653–3.733, and 3.896–3.921, for $X = 2, 3, 4$, respectively.

Finally, it should be mentioned that some preliminary investigations carried out on the $Li_6(C_{5v})$ cluster (see Chart) have shown that non-nuclear maxima occur on the triangular faces of the pentagonal pyramid, a result confirming the conclusions drawn for the planar clusters, despite the presence in Li_6 (C_{5v}) of the apical atom characterized by high connectivity index and, probably, by an unusual formal valence.

Appendix

The theory of molecular structure has been discussed extensively in literature (see for instance [18a, b]). Here we summarize only the essential points which are pertinent to the discussion of our results and which were not anticipated in the text.

In Table A1 are collected the main parameters used in the topological analysis and their corresponding notations.

Table A1. Definition of the main parameters used in the topological analysis of electron density[a]

Parameter	Density parameters
$\rho(\boldsymbol{r})$	Electron density at the point $\boldsymbol{r}$
λ_i	Principal curvatures (eigenvalues of M) of ρ at critical points ($\lambda_1 \leq \lambda_2 \leq \lambda_3$)
ε	Ellipticity (anisotropy) of ρ at bond critical point; $\varepsilon = (\lambda_1/\lambda_2) - 1$; λ_1 and λ_2 are principal curvatures perpendicular to the bond path
$-\nabla^2\rho(\boldsymbol{r})$	Negative of the Laplacian of $\rho(\boldsymbol{r})$
μ_i	Principal curvatures μ_i of $-\nabla^2\rho$ at a critical point of the $-\nabla^2\rho(\boldsymbol{r})$ scalar field ($\mu_1 \leq \mu_2 \leq \mu_3$)
$G(\boldsymbol{r})$	Local kinetic energy density at $\boldsymbol{r}$; $G(\boldsymbol{r}) = \frac{1}{2}\nabla\nabla'\Gamma^1(\boldsymbol{r}, \boldsymbol{r}')\|_{\boldsymbol{r}=\boldsymbol{r}'}$ where $\Gamma^1(\boldsymbol{r}, \boldsymbol{r}')$ is the one-particle density matrix
$H(\boldsymbol{r})$	Local energy density at $\boldsymbol{r}$; $H(\boldsymbol{r}) = G(\boldsymbol{r}) + V(\boldsymbol{r})$ where $V(\boldsymbol{r})$ is the local potential energy density
M	Hessian matrix of ρ

[a] The symbols related to the integrated properties are reported in Table 5

The molecular charge distribution is described by the scalar function $\rho(\boldsymbol{r}, \boldsymbol{X})$, where $\boldsymbol{r}$ is a vector in the ordinary three-dimensional space R^3 and $\boldsymbol{X}$ represents any set of nuclear coordinates in the space of nuclear configurations R^q. The chemical structure of a molecule can be unambigously assigned by determining number and kind of *critical points* of its electronic charge distribution, that is the points where the gradient of ρ (the vector $\nabla\rho$ of the first derivatives of ρ) vanishes. The collection of the second derivatives of ρ, evaluated at the critical point $\boldsymbol{r}_c$ defines the real 3×3 symmetric Hessian matrix. The principal curvatures of ρ at $\boldsymbol{r}_c$ (i.e. the eigenvalues of the Hessian, λ_i, ($\lambda_1 \leq \lambda_2 \leq \lambda_3$)) define the rank p and the signature q at the critical point (p, q). The rank of a critical point is given by the number of non-zero eigenvalues, and its signature is the algebraic sum of their signs.

There are only four possible non-degenerate critical points in R^3, namely $(3, -3)$, $(3, -1)$, $(3, +1)$, and $(3, +3)$. The critical points of the type $(3, +3)$ and $(3, -3)$ are associated with a local minimum and a local maximum in $\rho(\boldsymbol{r})$, respectively. With some important exceptions (see Text) a local maximum in $\rho(\boldsymbol{r})$ can occur only at the position of a nucleus. The collection of all integral curves (named *gradient paths*) $\boldsymbol{r}(S) = \boldsymbol{r}_0 + \int_0^S \nabla\rho\,[\boldsymbol{r}(t), \boldsymbol{X}]\,dt$ which are solutions of the differential equation $d\boldsymbol{r}(S)/dS = \nabla\rho\,[\boldsymbol{r}(S), \boldsymbol{X}]$ for some initial value $\boldsymbol{r}(0) \equiv \boldsymbol{r}_0$, and which in general will terminate at a given $(3, -3)$ critical point, defines a subspace in R^3, which is the *basin* of that critical point. Therefore, the $(3, -3)$ critical point (usually a nucleus) acts as an *attractor* for its basin. The union of a nucleus and its basin defines an *atom* in the molecule.

Two adjacent basins are separated by an interbasin surface $S(\boldsymbol{r})$, through which the gradient vector field of ρ has zero flux (i.e. $\nabla\rho(\boldsymbol{r}) \cdot \boldsymbol{n}(\boldsymbol{r}) = 0$, $\forall \boldsymbol{r} \in S(\boldsymbol{r})$, where $\boldsymbol{n}(\boldsymbol{r})$ is the unit vector normal to the surface at $\boldsymbol{r}$).

Due to its zero-flux properties, any interbasin surface is generated by the gradient paths which terminate at a critical point contained in the same surface. This is a $(3, -1)$ critical point, i.e. a two dimensional attractor, and is called a bond critical point (BCP). In fact, the eigenvector of the positive curvature at BCP gives the initial direction of two gradient paths which terminate at two neighboring $(3, -3)$ attractors, thus defining a *bond path*. Along a bond path ρ is maximum with respect to any lateral displacement.

The existence of a bond path linking two $(3, -3)$ attractors is a necessary condition for the existence of a bond between the two attractors. The network of bond paths for a molecule in a given nuclear configuration defines the *molecular graph*. This latter describes a topological structure that is usually in one-to-one correspondence with chemical bond networks commonly drawn (at least for conventional chemical systems).

Also the critical points of the type $(3, +1)$ and $(3, +3)$ have a chemical meaning. The eigenvectors associated with the two positive eigenvalues of the Hessian matrix evaluated at a $(3, +1)$ critical point

generate a surface (named *ring surface*) in which the (3, +1) critical point (*ring critical point*) is a minimum in ρ. The axis perpendicular to the ring surface at the ring critical point, along which $\rho(\boldsymbol{r})$ is a maximum, is the intersection of the boundaries of the atomic basins forming the ring (see Figs. 4–6).

Finally, the (3, +3) critical point is associated with the minimum in the charge density inside a cage. A (3, +3) critical point, a *cage critical point*, is common to all the interatomic surfaces of atoms forming the cage.

The properties of ρ at BCPs allows a quantitative analysis of the characteristics of a bond. The ρ values at BCP correlate with bond lengths [37] and bond orders. These relationships have been proposed in particular for C–C bonds in organic molecules [26, 37].

Very useful information on the shape of the charge distribution along the bond is given by the principal curvatures (λ_i) of ρ at BCP. The asymmetry of the charge distribution in a plane perpendicular to the bond path may be appreciated considering the ratio $\varepsilon = (\lambda_1/\lambda_2) - 1$ of the two negative curvatures of ρ at the BCP. The ε quantity, called *ellipticity* of the bond, gives a measure of the deviation of the charge distribution from cylindrical symmetry and thus is correlated with the amount of π character of a bond [26].

The total charge density normally exhibits local maxima only at the positions of nuclei and its topology, while providing the basis for the definition of atoms and molecular structure, gives no indication of concentration of charge as anticipated in terms of the Lewis electron pair model or localized orbital models of electronic structure.

A scalar field (such as $\rho(\boldsymbol{r}, \boldsymbol{X})$) is *concentrated* in those regions of space where its Laplacian is negative and *depleted* in those where it is positive. Therefore, the Laplacian of the charge density, the quantity $\nabla^2\rho(\boldsymbol{r}) = \sum_{j=1,3} \partial^2\rho(\boldsymbol{r})/\partial x_j^2$, determines the regions of space wherein electronic charge is locally concentrated or depleted. The form of the Laplacian of ρ for an isolated atom reflects its shell structure since it exhibits a corresponding number of pairs of spherical shell of alternating charge concentration and charge depletion (the inner shell of each pair being always the region of charge concentration) [36].

The *valence shell of charge concentration* (VSCC) of an isolated atom possesses a spherical surface over which the charge is maximally concentrated (for each point of this surface $\nabla(-\nabla^2\rho) = 0$, and each point on this surface is a (1, −1) critical point; two of the curvatures of $-\nabla^2\rho$ are zero and the third curvature, the one along a radial line, is negative). The VSCC of an isolated atom is disturbed upon chemical combination through the creation of local maxima and local minima in $-\nabla^2\rho$ all keeping in the neighbourhood of the "atomic" spherical surface of maximum concentration. The numbers, location and relative sizes of the bonded and nonbonded concentration of charge in VSCC for a bounded atom are found to be in general agreement with the corresponding properties that are ascribed to bonded and nonbonded electron pairs in models of electronic structure. It is important to note that stationary points in the Laplacian of ρ *do not determine maxima or minima in* ρ *itself*, but rather the points where the electronic charge *is locally compressed* ($\nabla^2\rho < 0$) *or expanded* ($\nabla^2\rho > 0$).

The critical point of the Laplacian of ρ are classified in the same way as the ρ critical points, through the analysis of the rank and signature of the eigenvalues (μ_i, $i = 1-3$) of the Hessian of $-\nabla^2\rho$.

A second point is of interest [18c, 36]. Due to the local (pointwise) form of the virial theorem

$$(h^2/4m)\nabla^2\rho(\boldsymbol{r}) = V(\boldsymbol{r}) + 2G(\boldsymbol{r})$$
$$H(\boldsymbol{r}) = V(\boldsymbol{r}) + G(\boldsymbol{r})$$

it is possible to *associate* regions where the charge is locally concentrated with regions where the *stabilizing contributions of the potential energy are dominant.* In the above equation $V(\boldsymbol{r})$ and $G(\boldsymbol{r})$ provide the potential and the kinetic energy of the atom in molecule when integrated in the atomic basin or of the molecule itself, when integrated over the overall molecular space. $H(\boldsymbol{r})$ is the local energy density.

So the possibility to relate regions of concentration and depletion of charge with corresponding regions of dominant potential energy decrease and kinetic energy increase, respectively, form a basis for the classification of atomic interactions [18c]. Interactions resulting from sharing of charge density

between atoms (covalent and polar bonds) are characterized by *dominant negative curvatures* of ρ in direction perpendicular to the line of interaction, concentration of charge in the internuclear region and $\nabla^2\rho < 0$, so indicating that the potential energy contribution to the virial from this region is greater than the contribution from the kinetic energy.

Interactions between closed-shell atoms (ionic bonds, hydrogen bonds, Van der Waal's molecules) are governed by the contraction of charge toward each of the interacting nuclei, with consequent dominant positive curvature of ρ in direction parallel to the line of interaction. Electronic charge is depleted in the interatomic surface, $\nabla^2\rho > 0$ and the mechanics of interaction is characterized by the relative large value of the kinetic energy, particularly the component parallel ($G_{\|}$) to the interaction line. So the regions of dominant potential energy contributions are separately localized within the boundaries of each of the interacting atoms or molecules.

References and notes

1. Koutecký J & Fantucci P (1986) Chem Rev 86:539
2. Morse MD (1986) Chem Rev 86:1049
3. Fantucci P, Balzarini P (1978) J Mol Catal 4:337
4. Beckmann HO, Koutecký J, Botscwhina P, Meyer W (1979) Chem Phys Lett 67:119
5. Beckmann HO, Koutecký J, Bonacic-Koutecký V (1980) J Chem Phys 73:5182
6. Flad J, Stoll H, Preuss H (1979) J Chem Phys 71:3042
7. Martins JL, Buttet J, Car R (1984) Phys Rev 53:655; Martins JL, Buttet J (1985) Phys Rev B 31:1804
8. Rao KB, Jena P (1985) Phys Rev B 32:2058
9. Ray AK, Fry JL, Myles CW (1985) J Phys B 18:381
10. Boustani I, Pewestorf W, Fantucci P, Koutecký J, Bonacic-Koutecký V (1987) Phys Rev B 35:9437
11. Koutecký J, Fantucci P (1986) Z Phys D 3:147
12. Pacchioni G, Plavsic D, Koutecký J (1983) Ber Bunsenges Phys Chem 87:503
13. Plavsic D, Koutecký J, Pacchioni G, Bonacic-Koutecký V (1983) J Phys Chem 87:1096
14. Fantucci P, Koutecký J, Pacchioni G (1984) J Chem Phys 80: 325
15. McAdon MH, Goddard III WA (1985) Phys Rev Lett 55:2563; McAdon MH, Goddard III WA (1985) J Non Cryst Solids 75: 149; McAdon MH, Goddard III WA (1987) J Phys Chem 91:2607
16. Koutecký J, Pacchioni G, Jeung GH, Hass EC (1985) Surf Sci 156:650
17. Schwarz WHE, Valtazanos P, Ruedenberg K (1985) Theor Chim Acta 68:471
18. (a) Bader RFW, Nguyen-Dang TT (1981) Adv Quantum Chem 14:63 (b) Bader RFW, Nguyen-Dang TT, Tal Y (1981) Rep Prog Phys (1981) 44:893; (c) Bader RFW, Essen H (1984) J Chem Phys 80:1943
19. Besnainou S, Roux M, Daudel R, Compt Rend (1955) 241:311
20. Beckmann HO, Koutecký J (1982) Surf Sci 120:127 and references therein
21. Clementi E, Corongiu G (1982) Chem Phys Lett 90:359. The geometrical basis set for Li [13*s*] has been augmented by a more contracted and a more diffuse *s* function; the 2*p* and 3*d* exponents are the same of basis *B* and *C*. The corresponding energy of Li(^2S), −7.4326766 au, has to be compared with the HF limit value −7.4327257 au (Clementi E, Roetti C (1974) At Data Nucl Data Tables 14:177)
22. (a) Buenker RJ Peyerimhoff SD (1974) Theor Chim Acta 35:33; (b) Buenker RJ, Peyerimhoff SD, Butscher W (1978) Mol Phys 35:771; (c) Buenker RJ (1980) In: Burton PG (ed) Proceedings of the Workshop on Quantum Chemistry and Molecular Physic. Woollongong, Australia; (d) Buenker RJ (1982) Studies in physical and theoretical chemistry vol 21. Elsevier, Amsterdam; (e) Buenker RJ, Phillip RA (1985) J Mol Struct 123:291
23. (a) Biegler-König FW, Bader RFW, Tang T (1982) J Comput Chem 13:317; (b) An AIMPAC modified version for GOULD-SEL computers was actually used (Gatti C unpublished work)
24. A basin is defined as the region enclosed by all the gradient paths (traced out by following the gradient vector of ρ from some intial point) which terminate at the attractor (see Appendix)
25. It is interesting to note that also the ground state $X\ ^1\Sigma_g^+$ of C_2 exhibits a maximum at the C-C midpoint, at variance with the corresponding bonds in saturated and unsaturated hydrocarbons, which all show the usual (3, −1) bond critical point (an exceptional maximum in C_2H_2 $X\ ^1\Sigma_g^+$ disappears after the inclusion of electron correlation at the SD CI 6-31G** level [27a]). However,

the ρ_M/ρ_S value (see text) is exceedingly small (1.008) (MRD CI optimal geometry, including HF canonical valence and virtual orbitals in the active space and employing [9*s*5*p*1*d*/4*s*2*p*1*d*] [27b] basis set) and the maximum could be perhaps removed considering a wavefunction of even higher quality

26. Bader RFW, Slee TS, Cremer D, Kraka E (1983) J Am Chem Soc 105:5061
27. a) Gatti C, Bader RFW, MacDougall PJJ: J Chem Phys, submitted; b) Dunning TH (1970) J Chem Phys 53:2823; the *d* exponent was taken from [16]
28. Actually the two maxima do not normally coincide in location (see Appendix); for example, by lengthening the Li-Li bond to 6 au, a (3, −1) point in $-\nabla^2\rho$ is created at the ρ maximum located at the Li-Li midpoint, while the $-\nabla^2\rho$ bonded maximum remains nearly fixed at a distance of 2.55 au from Li (Table 4)
29. (a) Wiberg KB, Bader RFW, Lau CDH (1987) J Am Chem Soc 109:1001; (b) Bader RFW, Larouche A, Gatti C, Carroll MT, MacDougall PJ, Wiberg KB (1987) J Chem Phys 87:1142
30. The charge density values at the non-nuclear maximum and at its closest saddle point (labelled as 3 in Fig. 4a) are very similar for Basis *B* (1.13 and 1.12 au, respectively). This fact could suggest that a singularity in ρ is forming and that a structure change is at hand [18b, 31]. However, this is not the case as the softest in-plane curvatures of the charge density at the two critical points are associated with principal axes which are orthogonal to the line joining the two critical points
31. (a) Gatti C, Barzaghi M, Simonetta M (1985) J Am Chem Soc 107:878; b) Simonetta M, Barzaghi M, Gatti C (1986) J Mol Struct 138:39
32. Wiberg KB, Bader RFW, Lau CDH (1987) J Am Chem Soc 109:985
33. The substantial in-plane bond ellipticity of cyclopropane, which resembles in some respect the case of the central region of Li_4, provides a physical basis for its peculiar π functionality [26]
34. Moments other than the monopole (the net charge) may be determined for an atom in a molecule by averaging the corresponding operator over the charge density on the subspace. Here we are interested with the diagonal components of the traceless quadrupole moment tensor, defined as

$$Q_{ii}(\Omega) = -e \int_{\Omega} \rho(3i^2 - r^2)\, d\tau, \qquad i = x, y, z.$$

For a spherical distribution, the Q_{ii} are identically equal to zero, while a negative Q_{ii} value agrees with an accumulation of charge in the *ii* direction at the expense of the direction(s) associated with a positive Q_{jj} component

35. The bond paths which connect Li(4*nn*) to the non-nuclear attractors 2 and the non-nuclear attractors among themselves, form a four-membered ring, enclosing a surface within which the charge density attains a minimum value at the (3, +1) critical point (labelled as 8 in Fig. 5a). The principal axis associated with the λ_1 curvature of the ring critical point gives the direction of the line shared by the boundary surfaces of the three non-nuclear and Li(4*nn*). Two other three-membered rings are recognizeable in Fig. 5a, having as vertices a Li(3*nn*), a non-nuclear attractor like 2 and the non-nuclear attractor 1 which is in common to the two rings
36. These arguments are thoroughly discussed by Bader RFW, MacDougall PJ, Lau CDH (1984) J Am Chem Soc 106:1594
37. Cremer D, Kraka E, (1984) Croat Chem Acta 57:1265